Available online at www.sciencedirect.com
SCIENCE DIRECT®
C. R. Mecanique 334 (2006) 151–157
COMPTES RENDUS MECANIQUE
http://france.elsevier.com/direct/CRAS2B/

Porous polycrystals built up by uniformly and axisymmetrically oriented needles: homogenization of elastic properties

Andreas Fritsch [a,*], Luc Dormieux [b], Christian Hellmich [a]

[a] *Institute for Mechanics of Materials and Structures, Vienna University of Technology (TU Wien), 1040 Vienna, Austria*
[b] *LMSGC, UMR 113, CNRS/ENPC/LCPC, 77455 Marne-la-Vallée, France*

Received 20 January 2006; accepted 31 January 2006

Available online 10 March 2006

Presented by André Zaoui

Abstract

Porous polycrystal-type microstructures built up of needle-like platelets or sheets are characteristic for a number of biological and man-made materials. Herein, we consider (i) uniform, (ii) axisymmetrical orientation distribution of linear elastic, isotropic as well as anisotropic needles. Axisymmetrical needle orientation requires derivation of the Hill tensor for arbitrarily oriented ellipsoidal inclusions with one axis tending towards infinity, embedded in a transversely isotropic matrix; therefore, Laws' integral expression of the Hill tensor is evaluated employing the theory of rational functions. For a porosity lower 0.4, the elastic properties of the polycrystal with uniformly oriented needles are quasi-identical to those of a polycrystal with solid spheres. However, as opposed to the sphere-based model, the needle-based model does not predict a percolation threshold. As regards axisymmetrical orientation distribution of needles, two effects are remarkable: Firstly, the sharper the cone of orientations the higher the anisotropy of the polycrystal. Secondly, for a given cone, the anisotropy increases with the porosity. Estimates for the polycrystal stiffness are hardly influenced by the anisotropy of the bone mineral needles. Our results also confirm the very high degree of orientation randomness of crystals building up mineral foams in bone tissues. ***To cite this article: A. Fritsch et al., C. R. Mecanique 334 (2006).***

Résumé

Polycristaux poreux constitués d'aiguilles orientées de façon uniforme ou axisymétrique : homogénéisation des propriétés élastiques. De nombreux matériaux biologiques ou manufacturés présentent une microstructure poreuse à morphologie polycristalline constituée de feuillets ou d'aiguilles. On s'intéresse ici à des cristaux solides élancés, doués d'un comportement linéaire élastique isotrope ou anisotrope, dont les orientations sont distribuées de façon uniforme ou axisymétrique. Dans ce dernier cas, l'approche micromécanique proposée fait appel à la connaissance du tenseur de Hill pour une inclusion ellipsoidale d'élancement infini plongée dans un milieu isotrope transverse. L'expression intégrale de ce dernier donnée par Laws est évaluée numériquement en employant la théorie des fonctions holomorphes. Pour une porosité inférieure à 0,4, les propriétés élastiques du polycristal estimées à partir d'un schéma basé sur des inclusions ellipsoidales sont très proches de celles obtenues avec un schéma basé sur des inclusions sphériques. En revanche, à la différence du schéma basé sur des inclusions sphériques, le schéma basé sur des inclusions ellipsoidales ne prédit pas de seuil de percolation. En ce qui concerne la situation d'une distribution axisymétrique des orienta-

* Corresponding author.
E-mail addresses: andreas.fritsch@tuwien.ac.at (A. Fritsch), dormieux@lmsgc.enpc.fr (L. Dormieux), christian.hellmich@tuwien.ac.at (Ch. Hellmich).

1631-0721/$ – see front matter
doi:10.1016/j.crme.2006.01.008

tions des cristaux solides, deux effets méritent d'être soulignés. D'une part, l'anisotropie est d'autant plus marquée que l'angle du cône des orientations diminue. D'autre part, à angle de cône donné, l'anisotropie augmente avec la porosité. Les estimations de l'élasticité du polycristal sont très faiblement affectées par l'anisotropie du minéral osseux. Ces résultats confirment le caractère très largement désordonné de l'orientation des cristaux constituant des mousses minérales dans les tissus osseux. ***Pour citer cet article : A. Fritsch et al., C. R. Mecanique 334 (2006).***

Keywords: Biomechanics; Porous polycrystal; Orientation distribution; Micromechanics; Hill tensor; Anisotropy

Mots-clés : Biomécanique ; Polycristal poreux ; Distribution des orientations ; Micromécanique ; Tenseur de Hill ; Anisotropie

1. Introduction

Porous polycrystal-type microstructures built up of needle-like platelets or sheets can be found in a number of biological and man-made materials such as bone [1,2] or eggs [3], or at the cement paste level of concrete [4]. We here deal with homogenization of their overall (linear) elastic properties, by means of self-consistent schemes. Thereby, the solid phase (needles) is represented by cylindrical inclusions (a cylinder being the limit case of a prolate spheroid with its long axis being very much larger than its spherical axis), and the (empty) pore inclusions (drained conditions) are spherical; extension to pressurized pores according to [5] is straightforward. Subsequently, we consider (i) uniform, (ii) axisymmetrical orientation distribution of isotropic as well as anisotropic needles with elasticity tensor $\mathbb{C}_s$.

2. Uniform orientation distribution of needles

Uniformly oriented needles result in isotropic elastic properties of the polycrystal. The corresponding stiffness estimate $\mathbb{C}^{\mathrm{SCS}}$ reads as

$$\mathbb{C}^{\mathrm{SCS}} = (1-\phi)\mathbb{C}_s : \left\langle \left[\mathbb{I} + \mathbb{P}^{\mathrm{SCS}}_{\mathrm{cyl}} : \left(\mathbb{C}_s - \mathbb{C}^{\mathrm{SCS}}\right)\right]^{-1} \right\rangle : \left\{ (1-\phi) \left\langle \left[\mathbb{I} + \mathbb{P}^{\mathrm{SCS}}_{\mathrm{cyl}} : \left(\mathbb{C}_s - \mathbb{C}^{\mathrm{SCS}}\right)\right]^{-1} \right\rangle + \phi \left(\mathbb{I} - \mathbb{P}^{\mathrm{SCS}}_{\mathrm{sph}} : \mathbb{C}^{\mathrm{SCS}}\right)^{-1} \right\}^{-1} \tag{1}$$

with

$$\left\langle \left[\mathbb{I} + \mathbb{P}^{\mathrm{SCS}}_{\mathrm{cyl}} : \left(\mathbb{C}_s - \mathbb{C}^{\mathrm{SCS}}\right)\right]^{-1} \right\rangle = \int_{\varphi=0}^{2\pi} \int_{\vartheta=0}^{\pi} \left[\mathbb{I} + \mathbb{P}^{\mathrm{SCS}}_{\mathrm{cyl}}(\vartheta,\varphi) \left(\mathbb{C}_s - \mathbb{C}^{\mathrm{SCS}}\right)\right]^{-1} \frac{\sin\vartheta \, \mathrm{d}\vartheta \, \mathrm{d}\varphi}{4\pi} \tag{2}$$

where $\mathbb{I}$, $I_{ijkl} = 1/2(\delta_{ik}\delta_{jl} + \delta_{il}\delta_{kj})$, is the fourth-order unity tensor, δ_{ij} is the Kronecker delta, ϕ denotes the porosity, $\mathbb{P}^{\mathrm{SCS}}_{\mathrm{sph}}$ and $\mathbb{P}^{\mathrm{SCS}}_{\mathrm{cyl}}$ are the fourth-order Hill tensors for spherical and cylindrical inclusions, respectively. The Hill tensor for spherical inclusions, $\mathbb{P}^{\mathrm{SCS}}_{\mathrm{sph}}$, is widely available in the open literature [6,7]. The components of the Hill tensor for cylindrical inclusions embedded in an isotropic medium are given for a base frame coinciding with the long axis of the cylinder [6]. Transformation of Hill tensors related to differently oriented cylindrical inclusions, to one reference frame can be expressed by Euler angles ϑ and φ, rendering $\mathbb{P} = \mathbb{P}^{\mathrm{SCS}}_{\mathrm{cyl}}(\vartheta,\varphi)$ in Eq. (2).

The numerical solution of (1) shows that the effective Young's modulus E^{SCS} is practically independent of the needles' Poisson's ratio ν_s.

The question arises whether uniform orientation of needles can be appropriately considered by representing the solid phase simply by spherical inclusions. The corresponding self-consistent estimate $\mathbb{C}^{\mathrm{SCS}}$ for identical shape and orientation of inclusions reads as (see, e.g., [8])

$$\mathbb{C}^{\mathrm{SCS}} = (1-\phi)\mathbb{C}_s : \left\{ \mathbb{I} + \mathbb{P}^{\mathrm{SCS}}_{\mathrm{sph}} : \left(\mathbb{C}_s - \mathbb{C}^{\mathrm{SCS}}\right) \right\}^{-1} \tag{3}$$

In case of an incompressible solid phase (with bulk modulus $k_s \to \infty$), (3) can be solved analytically:

$$\mu^{\mathrm{SCS}} = \mu_s \frac{3(1-2\phi)}{3-\phi}, \qquad k^{\mathrm{SCS}} = \frac{4(1-\phi)}{3\phi}\mu^{\mathrm{SCS}} \tag{4}$$

where k^{SCS} and μ^{SCS} are the effective bulk and shear moduli, and μ_s is the shear modulus of the isotropic solid. This scheme shows a percolation threshold exactly equal to $\phi = \frac{1}{2}$, for any value of the Poisson's ratio ν_s of the solid phase.

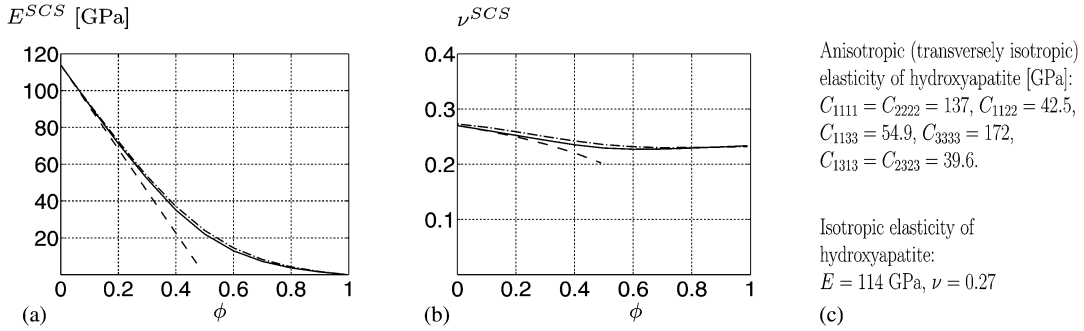

Fig. 1. (a) Young's modulus and (b) Poisson's ratio of isotropic porous polycrystals, predicted by the sphere-based and needle-based models, respectively (isotropic spheres … dashed lines, uniformly oriented isotropic needles … solid lines, uniformly oriented anisotropic needles … dash–dot lines); (c) Anisotropic and isotropic elasticity of hydroxyapatite [9].

As for a compressible solid phase, the homogenized Young's modulus E^{SCS} can still be approximated by the affine expression $E_s(1-2\phi)$ with an error of at most 4% relative to the exact solution, i.e., E^{SCS} is quasi-independent of Poisson's ratio.

On the entire porosity range, $0<\phi<1$, the self-consistent stiffness estimates based on uniformly oriented solid needles are quasi-identical for both isotropic and anisotropic needle behavior (Fig. 1 (a) and (b), see Fig. 1(c) for elastic constants [9] of hydroxyapatite crystals building up porous foams in bone [2]). In addition, on the interval $0<\phi<0.4$, these estimates are quasi-identical to those based on isotropic solid spheres [Fig. 1 (a) and (b)]. From a physical viewpoint, one may argue that, at a sufficiently high concentration, both spherical as well as isotropic or anisotropic needle-type particles build up similar contiguous matrices. Particularly, in the vicinity of $\phi=0$, the first-order expansions of the homogenized elastic constants with respect to the porosity are identical for the two models with an isotropic solid phase, reading as:

$$\frac{E^{\mathrm{SCS}}}{E_s}=1-\frac{3}{2}\frac{(1-\nu_s)(5\nu_s+9)}{7-5\nu_s}\phi;\qquad \nu_{\mathrm{SCS}}=\nu_s+\phi\frac{3(1-5\nu_s)(1-\nu_s^2)}{2(7-5\nu_s)} \tag{5}$$

$$\frac{k^{\mathrm{SCS}}}{k_s}=1-\frac{3}{2}\frac{1-\nu_s}{1-2\nu_s}\phi;\qquad \frac{\mu^{\mathrm{SCS}}}{\mu_s}=1-15\frac{1-\nu_s}{7-5\nu_s}\phi \tag{6}$$

However, as opposed to the sphere-based model, the needle-based model does not predict any percolation threshold, i.e., E^{SCS}, k^{SCS} and $\mu^{\mathrm{SCS}}\to 0$ only if the volume fraction of the solid phase becomes very small ($\phi\to 1$). From an intuitive viewpoint, this is consistent with the 'rice grain effect': As compared to spheres, needles are more likely to contact each other, especially at low volume fraction ($\phi\to 1$). A first-order expansion in the vicinity of $\phi=1$ of μ^{SCS} (resp. k^{SCS}) can be sought in the form $\mu^{\mathrm{SCS}}\sim m(1-\phi)$ [resp. $k^{\mathrm{SCS}}\sim k(1-\phi)$]. As regards isotropic needles, analytical expressions for m and k can be derived and proven to be independent of ν_s:

$$m=\frac{71-2\sqrt{79}}{1575},\qquad k=\frac{-8+2\sqrt{79}}{189} \tag{7}$$

Accordingly, the limit of ν^{SCS} when ϕ tends towards 1 is independent of ν_s as well:

$$\lim_{\phi\to 1}\nu^{\mathrm{SCS}}=\frac{17-\sqrt{79}}{35} \tag{8}$$

3. Axisymmetric orientation distribution of needles

Axisymmetrically oriented needles result in transversely isotropic elastic properties of the polycrystal. With ϑ being measured with respect to the symmetry axis of the orientation distribution, we consider (i) uniform needle distribution in the cone $[0,\vartheta_{\max}]$, and (ii) Gaussian needle distribution around $\vartheta_{\max}/2$ with standard deviation s_ϑ;

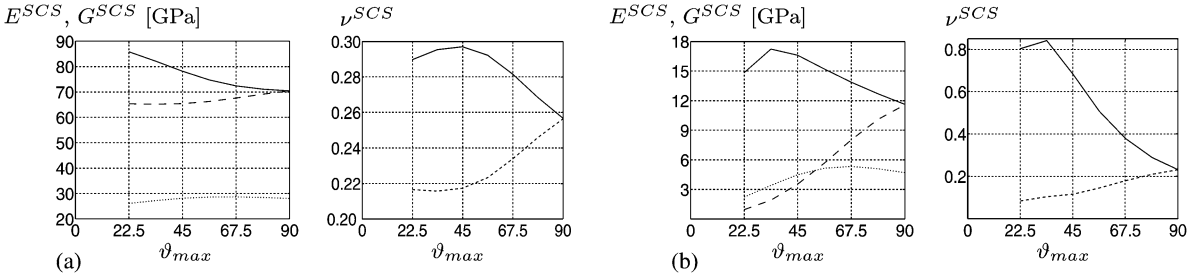

Fig. 2. Effect of axisymmetric distribution of anisotropic needles (uniformly distributed between $\vartheta = 0$ and $\vartheta = \vartheta_{\max}$) on the longitudinal and transverse Young's moduli, Poisson's ratios, and shear modulus for different porosities [(a) $\phi = 0.2$, (b) $\phi = 0.6$]. Longitudinal components are shown as solid lines, transversal components as dashed lines, and the shear modulus as dotted line.

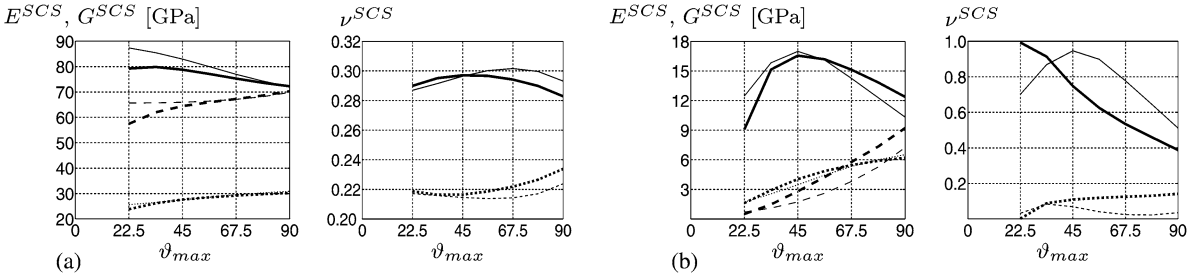

Fig. 3. Effect of axisymmetric distribution of anisotropic needles (Gaussian-type distributed around $\vartheta_{\max}/2$ with standard deviation s_ϑ) on the longitudinal and transverse Young's moduli and Poisson's ratios for different porosities [(a) $\phi = 0.2$, (b) $\phi = 0.6$] and different standard deviations ($s_\vartheta = 2.5^\circ \ldots$ thick lines, $s_\vartheta = 12^\circ \ldots$ thin lines). Longitudinal components are shown as solid lines, transversal components as dashed lines, and the shear modulus as dotted line.

both expressed in terms of a distribution function $F(\vartheta)$. The corresponding stiffness estimate still obeys (1), while (2) now reads as

$$\left\langle \left(\mathbb{I} + \mathbb{P}^{\mathrm{SCS}}_{\mathrm{cyl}} : \delta\mathbb{C}\right)^{-1} \right\rangle = \int_{\varphi=0}^{2\pi} \int_{\vartheta=0}^{\vartheta_{\max}} F(\vartheta) \left[\mathbb{I} + \mathbb{P}^{\mathrm{SCS}}_{\mathrm{cyl}}(\vartheta, \varphi)\left(\mathbb{C}_s - \mathbb{C}^{\mathrm{SCS}}\right)\right]^{-1} \frac{\sin\vartheta \, \mathrm{d}\vartheta \, \mathrm{d}\varphi}{2\pi(1 - \cos\vartheta_{\max})} \tag{9}$$

and while the Hill tensors $\mathbb{P}^{\mathrm{SCS}}_{\mathrm{cyl}}$ and $\mathbb{P}^{\mathrm{SCS}}_{\mathrm{sph}}$ now refer to inclusions in a transversely isotropic material.

Expressions for $\mathbb{P}^{\mathrm{SCS}}_{\mathrm{sph}}$ can be found in [1], and for determination of $\mathbb{P}^{\mathrm{SCS}}_{\mathrm{cyl}}$ we evaluate Laws' double integral expression of the Hill tensor [10] for arbitrarily oriented cylindrical inclusions embedded in a transversely isotropic material, employing the theory of rational functions. Thereby, we arrive at a single-integrated expression allowing for efficient computational evaluation (see Appendix A).

We evaluated Eq. (9) for a uniform distribution of needles between 0 and a maximum angle $\vartheta_{\max}$ as well as for a Gaussian distribution with different standard deviations around $\vartheta_{\max}/2$, see Figs. 2 and 3. Two effects are remarkable (Fig. 2): Firstly, as expected, the sharper the cone of orientations the higher is the anisotropy of the polycrystal. Secondly, the higher the porosity the more pronounced is the effect of the non-uniform needle orientation distribution, on both the Young's modulus and the Poisson's ratio. As compared to uniform needle distribution between $\vartheta = 0$ and $\vartheta = \vartheta_{\max}$, the Gaussian distribution around $\vartheta_{\max}/2$ with standard deviation s_ϑ significantly affects the effective Poisson's ratio (compare Figs. 2 and 3), while differences in Young's and shear moduli are, on the average, less than 7% for the investigated distributions (Figs. 2 and 3).

4. Discussion

The present results are also noteworthy from a biomechanical viewpoint: In the ultrastructure of bones and mineralized tissues hydroxyapatite crystals build up a contiguous network or mineral foam [2,1]. Single crystals have typical dimensions of 50 nm average length, 25 nm average width, and 1 to 7 nm thickness [11,12]. In a first approximation, they are often characterized as needles [12–14]. This renders the homogenization schemes developed here as

appropriate for mineral foams occurring in bones. In particular, agreement between homogenized elastic properties of uniformly oriented needles with those of spheres for a porosity lower 0.4 (Fig. 1) confirms the use of self-consistent schemes with spherical inclusions for hydroxyapatite polycrystals [1], which have been validated by the experimental data of [15,16]. At higher porosities, however, the needle-based scheme seems to be superior to the sphere-based scheme, since the former accounts for contiguity of the crystals, leading to non-zero homogenized stiffness, while the latter exhibits a percolation threshold beyond which the homogenized stiffness vanishes. Indeed, elasticity experiments [17] reveal that mineral crystals do contribute to the overall stiffness of low-mineralized turkey leg tendon, with a mineral foam porosity larger than 50%.

The present results also confirm the pronounced randomness of crystal orientation in bone tissues, revealed already by chemical [18] or mechanical [2] means: Any pronounced orientation of needles leads to high anisotropy ratios $E_{\text{tran}}/E_{\text{long}}$ far beyond two, and up to ten (Fig. 2). In real bone ultrastructure, however, this ratio lies always markedly below two [19,15,2].

Appendix A. Hill tensor for arbitrarily oriented cylindrical inclusions embedded in a transversely isotropic material

The starting point is Laws' classical expression for the Hill tensor (see for instance [10,20]):

$$\mathbb{P} = \frac{\omega_2\omega_3}{4\pi} \int\limits_{|\xi|=1} \frac{\boldsymbol{\Gamma}}{(\boldsymbol{\xi}\cdot\mathbf{A}^T\cdot\mathbf{A}\cdot\boldsymbol{\xi})^{3/2}}\,\mathrm{d}S(\boldsymbol{\xi}) \tag{A.1}$$

$\boldsymbol{\xi}$ is the unit length vector pointing from the origin of the sphere to the surface element $\mathrm{d}S(\boldsymbol{\xi})$. The second-order tensor $\mathbf{A}$ describes the shape of the ellipsoid, with base vectors $\mathbf{w}_1$, $\mathbf{w}_2$ and $\mathbf{w}_3$ pointing in the principal directions of the ellipsoid,

$$\mathbf{A} = \mathbf{w}_1\otimes\mathbf{w}_1 + \omega_2\mathbf{w}_2\otimes\mathbf{w}_2 + \omega_3\mathbf{w}_3\otimes\mathbf{w}_3, \quad \omega_3 \gg 1 \tag{A.2}$$

The fourth-order tensor $\boldsymbol{\Gamma}$ is defined as

$$\boldsymbol{\Gamma} = \boldsymbol{\xi} \overset{s}{\otimes} \mathbf{K}^{-1} \overset{s}{\otimes} \boldsymbol{\xi}, \quad \mathbf{K} = \boldsymbol{\xi}\cdot\mathbb{C}\cdot\boldsymbol{\xi} \tag{A.3}$$

The second-order tensor $\mathbf{K}$ is the acoustic tensor, $\mathbb{C}$ is the stiffness tensor of the transversely isotropic matrix. $\overset{s}{\otimes}$ denotes the symmetrized tensor product.

The technique presented hereafter adapts the ideas presented in [21] and [7] to cylindrical inclusions. First, we consider the denominator of expression (A.1). The unit vector $\boldsymbol{\xi}$ can be expressed in spherical coordinates $\Phi \in [0, 2\pi]$ and $\Theta \in [0, \pi]$ as $\xi_1 = \sin\Theta\cos\Phi$, $\xi_2 = \sin\Theta\sin\Phi$ and $\xi_3 = \cos\Theta$, so that $\mathrm{d}S = \sin\Theta\mathrm{d}\Phi\mathrm{d}\Theta$. Since

$$\boldsymbol{\xi}\cdot\mathbf{A}^T\cdot\mathbf{A}\cdot\boldsymbol{\xi} = \omega_3^2\cos^2\Theta + \sin^2\Theta\left(\cos^2\Phi + \omega_2^2\sin^2\Phi\right)$$

we find with $x = \cos\Theta$ and $\gamma^2 = \frac{1}{\omega_3^2}(\cos^2\Phi + \omega_2^2\sin^2\Phi)$

$$\mathbb{P} = \frac{\omega_2}{4\pi}\int\limits_0^{2\pi}\int\limits_{-1}^{1} \frac{\gamma^2}{[x^2+(1-x^2)\gamma^2]^{3/2}}\frac{\boldsymbol{\Gamma}(x,\Phi)}{\cos^2\Phi+\omega_2^2\sin^2\Phi}(-\mathrm{d}x)\,\mathrm{d}\Phi \tag{A.4}$$

Considering $\omega_3 \to \infty(\gamma \to 0)$, and use of the "Dirac delta function" $\delta(x)$

$$\lim_{\gamma\to 0}\frac{\gamma^2}{[x^2+(1-x^2)\gamma^2]^{3/2}} = 2\delta(x), \qquad \int \delta(x)f(x)\,\mathrm{d}x = f(0) \tag{A.5}$$

yields, with $\omega_2 = 1$,

$$\mathbb{P} = \frac{1}{2\pi}\int\limits_0^{2\pi}\boldsymbol{\Gamma}\left(\Theta=\frac{\pi}{2},\Phi\right)\mathrm{d}\Phi \tag{A.6}$$

Next, we consider the numerator of Eq. (A.1), $\boldsymbol{\Gamma} = \boldsymbol{\xi}\overset{s}{\otimes}\mathbf{K}^{-1}\overset{s}{\otimes}\boldsymbol{\xi}$. Expressing $\boldsymbol{\xi}$ and $\mathbf{K}$ in terms of the base vectors $\mathbf{w}_1$ and $\mathbf{w}_2$, while adopting $z = \cot\Phi$, yields

$$\boldsymbol{\xi} = \cos\Phi\mathbf{w}_1 + \sin\Phi\mathbf{w}_2 = \sin\Phi(z\mathbf{w}_1 + \mathbf{w}_2) \tag{A.7}$$

$$\mathbf{K} = \boldsymbol{\xi}\cdot\mathbb{C}\cdot\boldsymbol{\xi} = \sin^2\Phi\big((z\mathbf{w}_1+\mathbf{w}_2)\cdot\mathbb{C}\cdot(z\mathbf{w}_1+\mathbf{w}_2)\big)\sin^2\Phi\underbrace{\big(z^2\mathbf{Q} + z\big(\mathbf{R}+\mathbf{R}^T\big)+\mathbf{T}\big)}_{\mathbf{K}'(z)} \tag{A.8}$$

when having introduced the second-order tensors $\mathbf{Q}$, $\mathbf{R}$ and $\mathbf{T}$ as

$$\mathbf{Q} = \mathbf{w}_1\cdot\mathbb{C}\cdot\mathbf{w}_1, \qquad \mathbf{R} = \mathbf{w}_1\cdot\mathbb{C}\cdot\mathbf{w}_2, \qquad \mathbf{T} = \mathbf{w}_2\cdot\mathbb{C}\cdot\mathbf{w}_2 \tag{A.9}$$

$$\mathbf{K}(\Phi) = \sin^2\Phi\underbrace{\big(z^2\mathbf{Q} + z\big(\mathbf{R}+\mathbf{R}^T\big)+\mathbf{T}\big)}_{\mathbf{K}'(z)} \tag{A.10}$$

$\mathbf{K}'(z)$ is a second-order polynomial. In order to obtain the inverse of $\mathbf{K}'(z)$, we use the matrix of cofactors (algebraic complements) $\mathbf{co}\,\mathbf{K}'$,

$$\big(\mathbf{K}(z)\big)^{-1} = \frac{1}{\sin^2\Phi}\big(\mathbf{K}'\big)^{-1} = \frac{1}{\sin^2\Phi}\frac{1}{\det\mathbf{K}'}\big(\mathbf{co}\,\mathbf{K}'\big) \tag{A.11}$$

The determinant of $\mathbf{K}'$, $\det\mathbf{K}'$, is a sixth-order polynomial. Thus

$$\begin{aligned}\boldsymbol{\Gamma} &= \boldsymbol{\xi}\overset{s}{\otimes}\mathbf{K}^{-1}\overset{s}{\otimes}\boldsymbol{\xi} = \frac{1}{\sin^2\Phi}\frac{1}{\det\mathbf{K}'}\big(\boldsymbol{\xi}\overset{s}{\otimes}\big(\mathbf{co}\,\mathbf{K}'\big)\overset{s}{\otimes}\boldsymbol{\xi}\big)\\ &= \frac{1}{\sin^2\Phi}\frac{1}{\det\mathbf{K}'}\big(\sin^2\Phi(z\mathbf{w}_1+\mathbf{w}_2)\overset{s}{\otimes}\big(\mathbf{co}\,\mathbf{K}'\big)\overset{s}{\otimes}(z\mathbf{w}_1+\mathbf{w}_2)\big)\end{aligned} \tag{A.12}$$

Insertion of Eq. (A.12) into Eq. (A.6) and use of $\Phi = \operatorname{arccot} z$ yields

$$\mathbb{P} = \frac{1}{2\pi}\int_{\Phi=0}^{2\pi}\boldsymbol{\Gamma}\,\mathrm{d}\Phi = \frac{1}{2\pi}2\int_{z=-\infty}^{\infty}\boldsymbol{\Gamma}\frac{\mathrm{d}z}{1+z^2} \tag{A.13}$$

$$= \frac{1}{\pi}\int_{-\infty}^{\infty}\frac{(z\mathbf{w}_1+\mathbf{w}_2)\overset{s}{\otimes}(\mathbf{co}\,\mathbf{K}')\overset{s}{\otimes}(z\mathbf{w}_1+\mathbf{w}_2)}{(\det\mathbf{K}')(1+z^2)}\,\mathrm{d}z \tag{A.14}$$

The integrand in (A.14) is a rational fraction with a sixth-order polynomial in the numerator and an eighth-order polynomial in the denominator. Hence, the integration can be based on the Residue theorem:

$$\int_{-\infty}^{\infty} f(z)\,\mathrm{d}z = 2i\pi\sum_j \mathrm{Res}(f, z_j) \tag{A.15}$$

where z_j are the poles with a positive imaginary part, of the function $f(z)$.

References

[1] Ch. Hellmich, J.-F. Barthélémy, L. Dormieux, Mineral-collagen interactions in elasticity of bone ultrastructure—a continuum micromechanics approach, European Journal of Mechanics A—Solids 23 (2004) 783–810.

[2] Ch. Hellmich, F.-J. Ulm, Are mineralized tissues open crystal foams reinforced by crosslinked collagen?—some energy arguments, Journal of Biomechanics 35 (2002) 1199–1212.

[3] H. Silyn-Roberts, R.M. Sharp, Crystal growth and the role of the organic network in eggshell biomineralization, Proceedings of the Royal Society of London, Series B 227 (1248) (1986) 303–324.

[4] V. Baroughel-Bouny, Caractérisation des pâtes de ciment et des bétons—méthodes, analyse, interprétation (Characterization of cement pastes and concretes—methods, analysis, interpretations), Technical report, Laboratoire Central des Ponts et Chaussées, Paris, France, 1994 (in French).

[5] X. Chateau, L. Dormieux, Micromechanics of saturated and unsaturated porous media, International Journal for Numerical and Analytical Methods in Geomechanics 26 (2002) 831–844.

[6] J.D. Eshelby, The determination of the elastic field of an ellipsoidal inclusion, and related problems, Proceedings of the Royal Society of London, Series A 241 (1957) 376–396.

[7] A. Suvorov, G.J. Dvorak, Rate forms of the Eshelby and Hill tensors, International Journal of Solids Structures 39 (2002) 5659–5678.

[8] A. Zaoui, Matériaux hétérogènes et composites (Heterogeneous materials and composites), Lecture Notes from École Polytechnique, Palaiseau, France, 1997 (in French).
[9] J.K. Katz, K. Ukraincik, On the anisotropic elastic properties of hydroxyapatite, Journal of Biomechanics 4 (1971) 221–227.
[10] N. Laws, The determination of stress and strain concentrations at an ellipsoidal inclusion in an anisotropic material, Journal of Elasticity 7 (1) (1977) 91–97.
[11] S. Weiner, H.D. Wagner, The material bone: structure—mechanical function relations, Annual Review of Materials Science 28 (1998) 271–298.
[12] P. Fratzl, S. Schreiber, K. Klaushofer, Bone mineralization as studied by small-angle X-ray scattering, Connective Tissue Research 34 (4) (1996) 247–254.
[13] N. Sasaki, Orientation of mineral in bovine bone and the anisotropic mechanical properties of plexiform bone, Journal of Biomechanics 24 (1991) 57–61.
[14] P. Fratzl, N. Fratzl-Zelman, K. Klaushofer, G. Vogl, K. Koller, Nucleation and growth of mineral crystals in bone studied by small-angle X-ray scattering, Calcified Tissue International 48 (1991) 407–413.
[15] S. Lees, J.M. Ahern, M. Leonard, Parameters influencing the sonic velocity in compact calcified tissues of various species, Journal of the Acoustical Society of America 74 (1) (1983) 28–33.
[16] S. Lees, Considerations regarding the structure of the mammalian mineralized osteoid from viewpoint of the generalized packing model, Connective Tissue Research 16 (1987) 281–303.
[17] S. Lees, E.A. Page, A study of some properties of mineralized turkey leg tendon, Connective Tissue Research 28 (1992) 263–287.
[18] F. Peters, K. Schwarz, M. Epple, The structure of bone studied with synchrotron X-ray diffraction, X-ray absorption spectroscopy and thermal analysis, Thermochimica Acta 361 (2000) 131–138.
[19] S. Lees, J.D. Heeley, P.F. Cleary, A study of some properties of a sample of bovine cortical bone using ultrasound, Calcified Tissue International 29 (1979) 107–117.
[20] N. Laws, A note on penny-shaped cracks in transversely isotropic materials, Mechanics of Materials 4 (1985) 209–212.
[21] C. Gruescu, V. Monchiet, D. Kondo, Eshelby tensor for a crack in an orthotropic elastic medium, Comptes Rendus Mecanique 333 (6) (2005) 467–473.